Luminescent ruthenium(II) complexes used for the detection of 8-oxoguanine in the human telomeric sequence

Journal:	*Bioconjugate Chemistry*
Manuscript ID	Draft
Manuscript Type:	Article
Date Submitted by the Author:	n/a
Complete List of Authors:	Gillard, Martin; Université catholique de Louvain, Chemistry Bonnet, Hugues; Université Grenoble Alpes Lartia, Remy; Communaute d'Universites et Etablissements Universite Grenoble Alpes, Dpt of Molecular chemistry Yacoub, Hiba; Université Grenoble Alpes Dejeu, Jerome; Departement de Chimie Moleculaire, Biomolecular Engineering and Interadction Defrancq, Eric; Universite Grenoble Alpes, Departement de chimie moléculaire Elias, Benjamin; Universite catholique de Louvain, Institute of Condensed Matter and Nanosciences

Luminescent ruthenium(II) complexes used for the detection of 8-oxoguanine in the human telomeric sequence

Martin Gillard, † Hugues Bonnet, ‡ Rémy Lartia, ‡ Hiba Yacoub, ‡ Jérôme Dejeu, ‡,§ Eric Defrancq*‡ and Benjamin Elias*†

† Université catholique de Louvain (UCLouvain), Institut de la Matière Condensée et des Nanosciences (IMCN), Molecular Chemistry, Materials and Catalysis (MOST), Place Louis Pasteur 1, bte L4.01.02, B-1348 Louvain-la-Neuve, Belgium

‡ Université Grenoble-Alpes (UGA), Département de Chimie Moléculaire, UMR CNRS 5250, CS 40700, 38058 Grenoble, France

§ FEMTO-ST Institute, CNRS UMR-6174, Université de Bourgogne Franche-Comté, F-25000 Besançon, France

ABSTRACT: Detecting cancer at the early stage of the disease is crucial to keep the best chance for successful treatment. The recent development of genomic screening, a methodology that is addressed to asymptomatic patients presumably at risk of carcinogenesis, has stimulated the quest for new tools able to signal the level of risk. Carcinogenesis has been associated to chronic oxidative stress exceeding the antioxidant defenses and leading to critical genome alteration levels. The telomeric regions are presumably the most exposed to oxidative stress due to their high concentration of guanine (*i.e.* the easiest oxidizable nucleic base). Accumulation of 8-oxoguanine in telomeres, thus oxidative lesions, was reportedly associated with telomeric crisis and carcinogenesis. In this study, we report on the capacity of Ru(II) polyazaaromatic complexes to photoprobe 8-oxoguanine into the telomeric sequence with the view of developing new tools for cancer risk screening.

Introduction

Diagnosis of cancer currently focuses on detecting early carcinogenesis stage in patients to give them the best chance for successful treatment.[1] Unfortunately, in the case of aggressive tumours, the cancer has already reached an advanced stage when the first symptoms are detected. This has stimulated the development of screening methods based on different strategies than early diagnosis. Screening is more specifically addressed to apparently healthy and asymptomatic patients that are presumably having a high risk of carcinogenesis.[2] Efficient screening requires the development of new tests or examinations that can be used rapidly and easily. In this context, the detection of cellular oxidative stress signals is of major interest. [3] Indeed, chronic acute oxidative stress is a great contributor to the development of numerous diseases including cancer. It consists in the presence of a too high level of reactive oxygen species (ROS) exceeding the antioxidant defences of the organism. This can be attributed to diverse environmental and intrinsic factors.[4] Excess of ROS can cause irreversible oxidative damages to DNA, which is particularly critical at the level of telomeres as they play a pivotal role for genome stability and integrity. Studies in mouse models, human tissues and cell culture provided evidence that oxidative stress promote and accelerate telomere dysfunction.[5] The loss of telomeres maintenance was reported to contribute to ageing-related diseases, telomere crisis and carcinogenesis.[6] This can be explained by the high sensitivity of telomeres to ROS resulting from their high concentration in guanine, the easiest oxidizable nucleic base ($E_{G^{+}/G}$ = + 1.29 V vs NHE).[7] The guanine oxidation mainly leads to the formation of 8-oxoguanine (8-oxoG), the most studied DNA damage by far, which once persistent in telomeres promotes the above mentioned telomere loss and crisis.[8] The detection of telomeric 8-oxoG may lead to the development of new screening tools able to sense a risk of carcinogenesis at the earliest stage.[9]

The human telomeric DNA sequence (hTel) varies from 2-50 kilobases of approximately 300-8,000 repeats of the sequence (-TTAGGG-). As a result of their high concentration in guanines, telomeres can adopt a quadruple helix structure, namely G-quadruplex (G4) consisting in the assembly of four guanines forming a guanine quartet through Hoogsteen bonds.[10] Studies reporting on the impact of oxidative lesions on the human telomeric G4 DNA structure stability were recently reported.[11] The destabilizing effect on the G4 structure due to reduced hydrogen-bonding ability caused by the replacement of a guanine residue by 8-oxoG was evaluated. It appeared that the 8-oxoG position into the G4 structure has a major impact on its stability.[12] Many studies demonstrated the abilities of ruthenium (II) complexes as "DNA light switch" or as DNA specific sites photoprobes *in vitro* or *in cellulo*.[13, 14] In the present study, we aim at investigating the potential of Ru(II) polyazaaromatic complexes as 8-oxoG photoprobes in telomeric DNA and in duplex DNA. Complexes $[Ru(bpy)_2napp]^{2+}$ **1**, $[Ru(phen)_2cpip]^{2+}$ **2** and $[Ru(phen)_2salphen]^{2+}$ **3** (**Figure 1**) were chosen for their reported ability to discriminate DNA topologies (such as G4 DNA and DNA mismatches) thanks to their high luminescence sensitivity.[15, 16] We report on a brief description of the synthesis and the photophysical properties of compounds **1-3** along with a more detailed study of their 8-oxoG photoprobing capacities. This was achieved thanks to luminescence titrations using five different oligodeoxynucleotides (ODN's) that incorporate (or not) an 8-oxoG residue.

Three selected ODN's **hTel**, **hTel-oxoG21** and **hTel-oxoG10** are based on the human telomeric sequence. They fold into G4 architectures with **hTel-oxoG21** and **hTel-oxoG10** including an 8-oxoG at the outer or at the central quartet of the G4, respectively. The two others selected ODN's **HP** and **HP-oxoG** are G-rich sequences that fold into a duplex hairpin shape with **HP-oxoG** including an oxo-G residue in the middle of the helix.

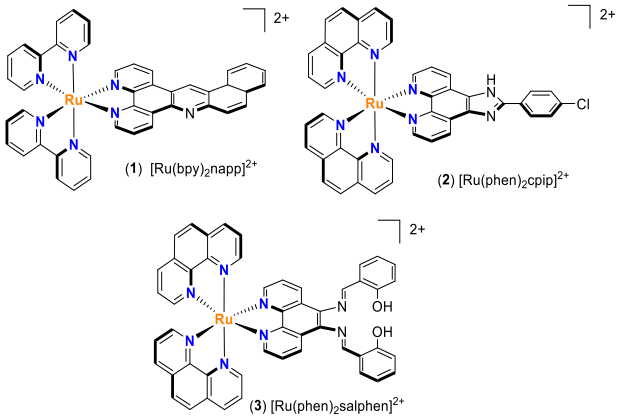

Figure 1. Structure of complexes $[Ru(bpy)_2napp]^{2+}$ **1**, $[Ru(phen)_2cpip]^{2+}$ **2** and $[Ru(phen)_2salphen]^{2+}$ **3**.

Results and Discussion

Synthesis

Complexes **1-3** were synthesized by the direct chelation of napp, cpip or salphen ligands onto $[Ru(bpy)_2Cl_2]$ or $[Ru(phen)_2Cl_2]$ using previously published methods.[15, 16] Complexes **1-3** were isolated as orange powders after purification on silica gel and were characterized by ^{1}H-NMR spectroscopy and HRMS. Compound **1** was also characterised by X-ray crystallography. The $[Ru(bpy)_3]^{2+}$ and $[Ru(phen)_3]^{2+}$ references were prepared and purified according to reported synthetic routes from the hydrated $RuCl_3$ salt.

Electrochemistry

In terms of electrochemical properties, compounds **1-3** display oxidation potentials that are very close to those of the reference compound $[Ru(bpy)_3]^{2+}$ (1.34 V vs Ag/AgCl). This corresponds to the Ru^{2+}/Ru^{3+} oxidation, which suggests that the HOMO of the compounds is metal centred (**Table 1**). Conversely, the potentials of first oxidation appear to be very different ranging from -0.77 V for complex **2** to -1.24 V for complex **1**. The strong influence of the extended ligand structure on the potential of first reduction of compounds **1-3** indicates that their LUMO orbitals lay on their extended ligands. It appears that the cpip ligand in complex **2** is responsible for a strong stabilization of the LUMO orbital compared to napp and salphen ligands in compounds **1** and **3**, which can be attributed to the strong electron stabilizing effect induced by the conjugated imidazole moiety. The next two reduction waves of compounds **1-3** all occur at very similar potentials to those of the reference complexes and correspond to the subsequent reductions of each bipyridine/phenanthroline ancillary ligands (-1.47 V and -1.71 V vs Ag/AgCl, for $[Ru(bpy)_3]^{2+}$).

Light absorption

The light absorption data of compounds **1-3** were recorded at ambient temperature in acetonitrile under air (**Figure 2** and **Table 2**). The absorption spectra are typical of Ru(II) complexes bearing polypyridyl ligands as described for $[Ru(bpy)_3]^{2+}$.[17] Comparison of the data obtained for **1-3** allows us to assign the strong UV absorption bands ($\varepsilon \approx 10^5$ $M^{-1}cm^{-1}$) to ligand-centred (LC) transitions. The band at *ca.* 285 nm in compound **1** and $[Ru(bpy)_3]^{2+}$ is attributed to the absorption of the bpy ligands while the band at *ca.* 265 nm in compounds **2** and **3** and in $[Ru(phen)_3]^{2+}$ is attributed to the phen ligands. The broad absorption bands at *ca.* 450 nm ($\varepsilon \approx 10^4$ $M^{-1}cm^{-1}$) result from metal-to-ligand charge-transfer (MLCT). Complex **1** displays the strongest visible light absorption ability (ε = 2.48 10^4 $M^{-1}cm^{-1}$ at 456 nm) among the reported compounds.

Table 2. Oxidation ($E_{1/2\ ox}$) and reduction ($E_{1/2\ red}$) potentials of complexes **1-3** and reference complexes.

Complex	$E_{1/2ox}$[a][V][b]	$E_{1/2\ red}$[a] [V][b]		
$[Ru(bpy)_3]^{2+}$	+ 1.34	-1.28	-1.47	-1.71
$[Ru(phen)_3]^{2+}$	+ 1.32	-1.30	-1.47	-1.68
$[Ru(bpy)_2napp]^{2+}$ **1**	+ 1.35	-1.24	-1.38	-1.65
$[Ru(phen)_2cpip]^{2+}$ **2**	+ 1.37	-0.77	- 1.43	-1.63
$[Ru(phen)_2salphen]^{2+}$ **3**	+1.36	-0.91	-1.45	-1.64

[a] Measured in dry acetonitrile. The electrochemical data for complexes $[Ru(bpy)_3]^{2+}$ and $[Ru(phen)_3]^{2+}$ are from references.[14, 17, 18]

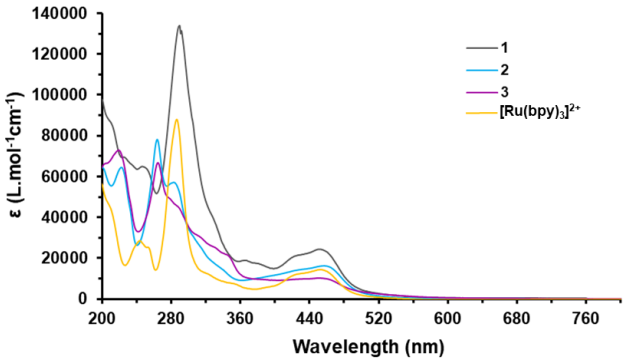

Figure 2. Absorption spectra of complexes **1-3** and $[Ru(bpy)_3]^{2+}$ in acetonitrile under air.

Table 1. Absorption data in CH_3CN for **1-3** and reference complexes.

Complex	Absorption λ_{max}[nm] (ε [10^4 $L.mol^{-1}.cm^{-1}$])[a]
$[Ru(bpy)_3]^{2+}$	250, 285 (8.71), 345 (sh), 452 (1.45)
$[Ru(phen)_3]^{2+}$	265, 287 (sh), 418 (sh), 447 (1.84)
$[Ru(bpy)_2napp]^{2+}$ **1**	246, 289 (13.6), 343 (sh), 456 (2.48)
$[Ru(phen)_2cpip]^{2+}$ **2**	265, 287 (sh), 335 (sh), 460 (1.61)
$[Ru(phen)_2salphen]^{2+}$ **3**	265, 288 (sh), 338 (sh), 458 (1.04)

[a] Measurements were performed with 1 x 10^{-5} mol L^{-1} solutions of the complex at room temperature. Extinction coefficients are reported in brackets. sh = shoulder. The absorption data for $[Ru(bpy)_3]^{2+}$ are from references. [14, 17, 18]

Light emission

The light emission properties of complexes **1-3** including their luminescence wavelengths, quantum yields and lifetimes were recorded in water and in acetonitrile and are gathered in **Table 3** along with those of $[Ru(bpy)_3]^{2+}$ and $[Ru(phen)_3]^{2+}$. Complexes **1-3** exhibit luminescence properties that are very close to those of the reference complexes $[Ru(bpy)_3]^{2+}$ and $[Ru(phen)_3]^{2+}$ with a broad unstructured emission at about 600 nm. The emission is also strongly dependent on the solvent polarity and relatively long (≈ microsecond) lifetimes of the excited states typical of ^{3}MLCT-emissive transition were measured. In addition, the bathochromic shift of the compounds' luminescence on going from acetonitrile to the more polar water and their large k_r values (> 10^4 s^{-1}) confirm the charge-separated excited states as reported for $[Ru(bpy)_3]^{2+}$ and $[Ru(phen)_3]^{2+}$.

Luminescence titrations

As mentioned in the introduction, ruthenium (II) complexes **1-3** were mainly selected for their reported abilities to photoprobe specific DNA topologies. While compound **1** has been previously reported to photodetect DNA mismatches, compounds **2** and **3** have been shown to act as G4 DNA photoprobes. This originates from the combination of (i) the high sensitivity of the polyazaaromatic Ru(II) complexes luminescence to the microenvironment with (ii) an appropriate structural design of the napp, cpip and salphen interacting ligands. In the present work, the ability of compounds **1-3** to photoprobe 8-oxoG lesions in G-quadruplex and in duplex DNA was assessed using five short ODN's. The **hTel-oxoG21** and **hTel-oxoG10** sequences were recently exploited by Podbevšek and co-workers and allowed to highlight the major impact of the 8-oxoG lesion localization on the conformation and stability of the resulting G4 structures.[12]

Table 1. Emission data in CH_3CN and H_2O at 298 K for complexes **1-3** and reference complexes.

Complex	Emission λ_{max} [a,b] [nm]		Φ_{em} [c,d]		τ_{em} [ns] [c]		k_r [10^3 s^{-1}]	
	CH_3CN	H_2O	CH_3CN	H_2O	CH_3CN	H_2O	CH_3CN	H_2O
$[Ru(bpy)_3]^{2+}$	604	604	0.062	0.042	855	630	77	69
$[Ru(phen)_3]^{2+}$	604	606	0.028	0.072	460	920	61	75
$[Ru(bpy)_2napp]^{2+}$ **1**	601	606	0.072	0.12	812	841	89	143
$[Ru(phen)_2cpip]^{2+}$ **2**	597	603	0.058	0.14	380	1315	152	106
$[Ru(phen)_2salphen]^{2+}$ **3**	599	600	0.018	0.075	688	1222	26	61

[a] Measurements made with air equilibrated solutions 5×10^{-6} mol.L^{-1} in complex. [b] λ_{exc} = 450 nm. [c] Measurements made with solutions 5×10^{-6} mol L^{-1} in complex under argon. [d] Measurements relative to $[Ru(bpy)_3]^{2+}$ in nitrogen purged aqueous solution (Φ_{em} = 0.063) or in nitrogen purged acetonitrile (Φ_{em} = 0.094).[19] The photophysical data for complexes $[Ru(bpy)_3]^{2+}$ and $[Ru(phen)_3]^{2+}$ are from references. [20]

They showed that the **hTel-oxoG10** G4 containing the 8-oxoG in the central G-quartet leads to structural rearrangement while the **hTel-oxoG21** G4 containing the 8-oxoG in the outer G-quartet retains the parent G4 fold. This may lead to differences in terms of interaction and luminescence properties in the presence of photoprobes **1-3**.

e increases of luminescence intensity in the presence of **hTel**, **hTel-oxoG21** and **hTel-oxoG10** are reported in **figure 4A** and allow to assess the photoprobing ability of compounds **1-3** for the different G4 folding sequences. As displayed in **figure 4B**, complexes **1-3** show very close increases of luminescence intensity in the presence of **hTel** and **hTel-oxoG21**, with complex **3** showing the strongest luminescence increase when interacting with G4 DNA (+224 and +247% in the presence of **hTel** and **hTel-oxoG21**, respectively). Conversely, the increase of luminescence intensity of complexes **1-3** appeared to be drastically reduced in the presence of the central 8-oxoG containing G4 structure **hTel-oxoG10**. Complex **2** revealed to be the best candidate to discriminate the central 8-oxoG containing G4 from the two other sequences (+72% vs +152-166%). A similar behaviour was observed for the duplex hairpin ODN's, as the increases of luminescence intensities of the three complexes **1-3** revealed to be significantly attenuated in the presence of the **HP-oxoG** against **HP**. Complex **1** revealed to be the most discriminant compound showing a fall of the luminescence increase from +494% vs **HP** to a weaker +177% vs **HP-oxoG**.

The dissociation equilibrium constants (K_D) values of the interaction between complexes **1-3** for the five DNA models were estimated using a modified McGhee-von Hippel model that fits the titration curves (**Table 4**).[20] The K_D values of the interaction of the compounds with the G4 DNA models **hTel, hTel-oxoG21** and **hTel-oxoG10** appear to be in the tenth of micromolar range. Each of the three complexes displays very close K_D values for the different studied sequences, ranging from 11 µM for compound **1** *vs* **hTel** to 43

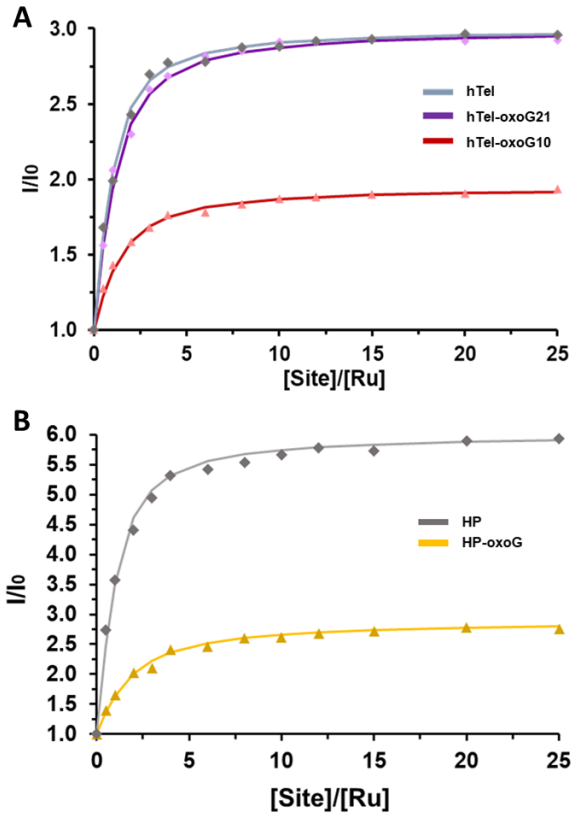

Figure 3. Relative luminescence intensity (I/I_0) of complex **1** as a function of the relative (**A**) G-quartet or (**B**) base pair concentration ([Site]/[Ru]) with I_0, the luminescence of the complex in the absence of DNA. Measurements were performed by using 2.5 µM of complex in 10 mM HEPES buffer, with 100 mM NaCl and 50 mM KCl at pH 7.4 under ambient air conditions. Excitation at 450 nm. The fitted curves were obtained by using a modified McGhee–von Hippel

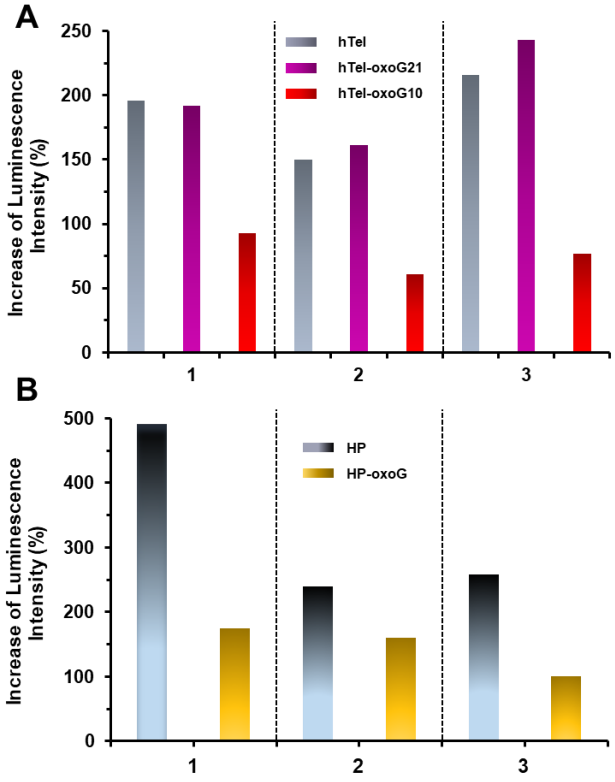

Figure 4. Increase of luminescence intensities (in %) for complexes **1-3** in the presence of (**A**) **hTel**, **hTel-oxoG21** and **hTel-oxoG10** and (**B**) **HP** and **HP-oxoG**. The results are reported as increase percentage compared to the luminescence of the complex in the buffer without DNA. Measurements were performed by using 2.5 µM of complex in 10 mM HEPES buffer, with 100 mM NaCl and 50 mM KCl at pH 7.4 under ambient air conditions.

Table 2. Binding affinity constants estimated for 1-3 with the five DNA models.

ODN	Constants	1	2	3
hTel	I/I_0 max	3.0	2.5	3.2
	K_D (μM)	11	14	23
hTel-oxoG21	I/I_0 max	2.9	2.6	3.4
	K_D (μM)	19	17	28
hTel-oxoG10	I/I_0 max	1.95	1.6	1.7
	K_D (μM)	22	31	43
HP	I/I_0 max	5.9	3.4	3.5
	K_D (μM)	12	205	176
HP-oxoG	I/I_0 max	2.7	2.6	2.0
	K_D (μM)	47	62	44

Binding constants were obtained by using a McGhee-von Hippel type equation; the binding site was fixed to two base pairs or to one G4 per complex (best fit). Errors are estimated to 5%.

μM for compound **3** *vs* **hTel-oxoG10**. The three compounds also display the same trend in terms of affinity for the three sequences with the affinity decreasing in this order: **hTel; hTel-oxoG21; hTel-oxoG10** (complex **1**: 11; 19; 22 μM, complex **2**: 14; 17; 31 μM and complex **3** 23, 28, 43 μM). The K_D values of the interaction of the complexes with the duplex DNA models **HP** and **HP-oxoG** are in the micromolar range for compound **1** and is one to two orders of magnitude higher for compounds **2** and **3** as previously reported. Complex **1** appears to be more affine for **HP** vs **HP-oxoG** (12 *vs* 47 μM) while compounds **2** (205 *vs* 62 μM) and **3** (176 *vs* 44 μM) are more affine for the 8-oxoG containing hairpin. The luminescence titration data demonstrate the very low impact of the presence of the 8-oxoG lesion on the interaction strength both for G4 and duplex HP type DNA. They also highlight the high sensitivity of the compounds to their local environment, especially when interacting with DNA. The ability of compounds **1-3** to photoprobe 8-oxo-G containing ODN's in **hTel-oxoG10** and **HP-oxoG** over their parent ODN's **hTel** and **HP** presumably arises from a poorer protection of the excited complexes in the 8-oxo-G containing ODN's towards non-radiative deexcitation sources. We assume this may result from the lower stability and consequent looser structure of **hTel-oxoG10** and **HP-oxoG** compared to **hTel** and **HP** respectively.

Bio-Layer interferometry studies

To further determine the affinities of complexes **1-3** for the different ODN's, we performed bio-layer interferometry analysis (BLI). This technique allows the determination of the association and dissociation kinetic constants between the compound of interest and its target, which directly gives access to the binding affinity/dissociation constant (such as surface plasmon resonance). BLI has been used to study biomolecular interactions between large biomolecules, such as protein–membrane, protein-carbohydrate interactions and more recently for the interactions of small molecules with G-quadruplex DNA.[15, 21] The studies were carried out in the same conditions than steady state luminescence titrations (10 mM HEPES pH 7.4, 100 mM NaCl, 50 mM KCl). BLI sensorgrams recorded for the interaction of complex **1** with the **hTel** and **hTel-oxoG10** are displayed in **Figure 5A** and in **Figure 5B**, respectively (see the supporting information for the other sensorgrams).As revealed by the fitting of the luminescence titration curves, compounds **1-3** exhibit

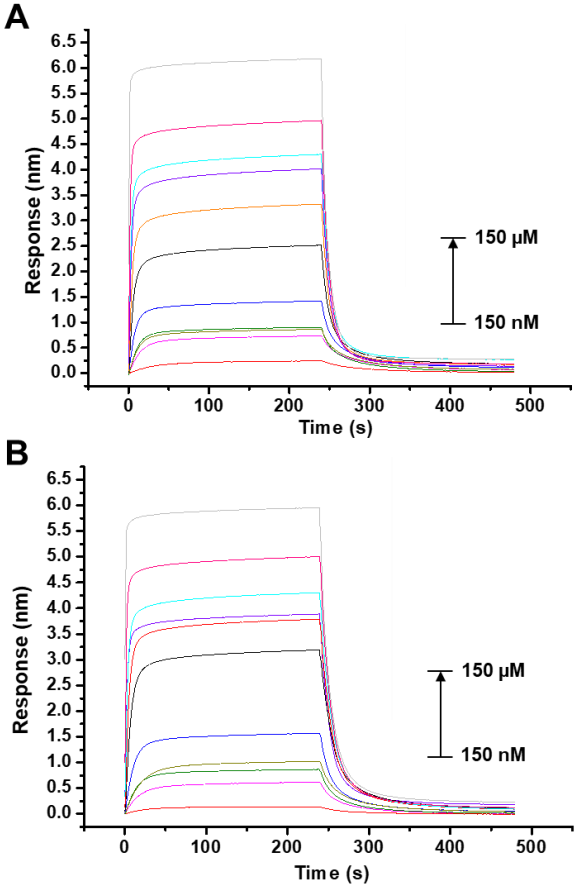

Figure 5 BLI response curves for the association and dissociation of complex **1** in the presence of **hTel** (A) and **hTel-oxoG10** (B). Measurements are performed using 0.15 to 150 μM of complex in 10 mM HEPES pH 7.4, 100 mM NaCl, 50 mM KCl.

Table 3. BLI analysis data for the interactions of complexes **1-3** with the studied ODN's.

ODN	Constant	1	2	3
hTel	k_{on} (10^3 M^{-1} s^{-1})	2.4 ± 0.7	1.1 ± 0.3	3.6 ± 1.1
	k_{off} (s^{-1})	50 ± 10	40 ± 20	47 ± 15
	K_D (μM)	19 ± 3	10 ± 5	15 ± 8
hTel-oxoG21	k_{on} (10^3 M^{-1} s^{-1})	2.9 ± 1.2	1.1 ± 0.2	4.4 ± 1.3
	k_{off} (s^{-1})	70 ± 20	6 ± 3	64 ± 20
	K_D (μM)	34 ± 8	7 ± 3	24 ± 11
hTel-oxoG10	k_{on} (10^3 M^{-1} s^{-1})	2.5 ± 0.9	0.8 ± 0.2	2.8 ± 1.2
	k_{off} (s^{-1})	80 ± 20	6 ± 2	78 ± 12
	K_D (μM)	33 ± 7	7 ± 2	35 ± 16
HP	k_{on} (10^3 M^{-1} s^{-1})	1.3 ± 0.3	n.d.[a]	2.0 ± 0.9
	k_{off} (s^{-1})	90 ± 10	n.d.[a]	100 ± 30
	K_D (μM)	82 ± 28	n.d.[a]	76 ± 16
HP-oxoG	k_{on} (10^3 M^{-1} s^{-1})	2.7 ± 0.9	n.d.[a]	1.4 ± 0.4
	k_{off} (s^{-1})	110 ± 40	n.d.[a]	148 ± 4
	K_D (μM)	73 ± 29	n.d.[a]	116 ± 34

Equilibrium dissociation constants were deduced from the kinetic rate constants. [a] Due to very low binding of the different complexes with hairpin DNA, the kinetics of the interactions could not be determined (n.d.) in the studied concentration range. Running buffer: 10 mM HEPES pH 7.4, 100 mM NaCl, 50 mM KCl. Measurements are performed using 0.15 to 150 μM of complex in 10 mM HEPES pH 7.4, 100 mM NaCl, 50 mM KCl.

K_D values in the tenth of micromolar range for their interaction with the different G4 folding ODN's **hTel**, **hTel-oxoG21** and **hTel-oxoG10** (**Table 5**). No consistent trend was observed neither for the kinetic k_{on} and k_{off} nor for the thermodynamic K_D constants that are comprised within a tight range (from 7 to 35 µM).

Conclusions

A series of three Ru(II) polyazaaromatic complexes were prepared. The compounds were selected as they were reported for their ability to photoprobe DNA specific sites thanks to their highly sensitive luminescence properties. A series of five ODN's that contain (or not) an 8-oxoG moiety were chosen and tested. This includes three G4 folding oligomers based on the human telomeric sequence, namely **hTel, hTel-oxoG21** and **hTel-oxoG10** and two duplex hairpin folding oligomers, namely **HP** and **HP-oxoG**. Steady state luminescence titrations revealed the ability of the three compounds to discriminate the **hTel-oxoG10** sequence that imbedded an 8-oxoG lesion into the G4's central quartet over the sequences **hTel** and **hTel-oxoG21** with respective luminescence increase of +72% *vs* +224-247% for the most discriminating complex. A similar trend was observed for the duplex hairpin **HP** that gave higher luminescence increases than for **HP-oxoG** (+494% vs **HP** to a weaker +177% vs **HP-oxoG**). The ability of the compounds **1-3** to photoprobe 8-oxo-G containing ODN's in **hTel-oxoG10** and **HP-oxoG** over their parent ODN's presumably arises from their lower ability to protect the compounds against non-radiative deexcitation sources (e.g. solvent collisions and oxygen sensitization). This probably results from the lower stability and consequent looser structure of **hTel-oxoG10** and **HP-oxoG**. Fitting of the luminescence titrations curves using a modified McGhee–von Hippel equation associated with results obtained from bio-layer interferometry studies allowed to make an in-depth study of the interaction between the complexes and the five ODN's. The results obtained showed that the compounds interact with the different ODN's within the tenth micromolar range for K_D values. They also highlighted that the presence of 8-oxoG had non-significant impact on the parameters of the interaction (k_{on}, k_{off} or K_D) of the complexes with both duplex hairpin and G4 folding sequences. Altogether, the results from luminescence titrations presented herein show promises for the development of sensitive photoprobes for the rapid detection and quantification of 8-oxoG in human telomeric DNA.

Experimental

Materials and instrumentation

$[Ru(bpy)_2Cl_2]$ and $[Ru(phen)_2Cl_2]$ precursors, napp, cpip and salphen ligands were synthesized according to previously described literature protocols. [15, 16] All solvents and reagents for the synthesis were of reagent grade and were used without any further purification. All solvents for the spectroscopic and electrochemical measurements were of spectroscopic grade. Water was purified with a Millipore Milli-Q system. Hairpin ODNs 29-mer **HP** ($^{3'}$CCGT(C)$_3$TACCG(T)$_5$CGGTA(G)$_3$ACGG$^{5'}$) and **HP-oxoG** ($^{3'}$CCGT(C)$_3$TACCG(T)$_5$CGGTA/^{oxo}G/GGACGG$^{5'}$) were purchased from Eurogentec. G4 ODNs 24-mer **hTel** ($^{3'}$A(GGGATT)$_3$GGGTT$^{5'}$), **hTel-oxoG21** ($^{3'}$AGG/^{oxo}G/ATT(GGGATT)$_2$GGGTT$^{5'}$), **hTel-oxoG10** ($^{3'}$A(GGGATT)$_2$G/^{oxo}G/GATTGGGTT$^{5'}$) were prepared by standard automated solid phase ODN synthesis on a 3400 DNA synthesizer. After purification by RP-HPLC, they were thoroughly desalted by size-exclusion chromatography (SEC). DNA and ODN concentrations were determined spectroscopically. Biotinylated ODN's were synthesized on a Controlled Pore Glass solid support by using the phosphoramidite approach with an Applied Biosystems 3400 DNA/RNA Synthesizer (1 □mol scale). ^{1}H NMR experiments were performed in $CDCl_3$, CD_3OD or CD_3CN on a Bruker AC-300 Avance II (300 MHz) or on a Bruker AM-500 (500 MHz) at 20 °C. The chemical shifts (given in ppm) were measured vs the residual peak of the solvent as the internal standard. High-resolution mass spectrometry (HRMS) spectra were recorded on a Q-Exactive orbitrap from ThermoFisher using reserpine as the internal standard. Samples were ionized by electrospray ionization (ESI; capillary temperature = 320 °C, vaporizer temperature = 320 °C, sheath gas flow rate = 5 mL min^{-1}).

Cyclic voltammetry was carried out in a one-compartment cell, using a glassy carbon disk working electrode (approximate area = 0.03 cm^2), a platinum wire counter electrode, and an Ag/AgCl reference electrode. The potential of the working electrode was controlled by an Autolab PGSTAT 100 potentiostat through a PC interface. The cyclic voltammograms were recorded with a sweep rate of 300 mV s^{-1}, in dried acetonitrile (Sigma-Aldrich, HPLC grade). The concentration of the complexes was 8×10^{-4} mol L^{-1}, with 0.1 mol L^{-1} tetrabutylammonium hexafluorophosphate as the supporting electrolyte. Before each measurement, the samples were purged by nitrogen.

UV/Vis absorption spectra were recorded on a Shimadzu UV-1700 spectrophotometer. Room temperature luminescence spectra were recorded on a Varian Cary Eclipse instrument. Luminescence intensity at 77 K was recorded on a FluoroLog 3 FL3-22 from Jobin Yvon equipped with an 18 V 450 W short-arc xenon lamp and an R928P photomultiplier, using an Oxford Instruments Optistat DN nitrogen cryostat controlled by an Oxford Intelligent Temperature Controller (ITC503S). Quantum yields were obtained using $[Ru(bpy)_3]^{2+}$ as a reference.[19] Luminescence lifetime measurements were performed after excitation at λ=450 nm obtained as the second harmonic of a titanium: sapphire laser (picosecond Tsunami laser Spectra at a repetition rate of 80 kHz. A Fluotime 200 instrument from AMS Technologies was used for the decay acquisition. It consists of a GaAs microchannel plate photomultiplier tube (Hamamatsu model R3809U-50) followed by a time-correlated single-photon counting system from Picoquant (PicoHarp300). The ultimate time resolution of the system is close to 4 ps. Luminescence decays were analyzed with FLUOFIT software available from Picoquant. Steady state luminescence titrations were performed in 10 mM HEPES pH 7.4, 50 mM NaCl and 100 mM KCl. The complex concentration was kept at 5 µM.

Bio-layer interferometry experiments were performed using sensors coated with streptavidin (SA sensors) purchased from Forte Bio (SARTORIUS). Prior to use, they were immersed for 10 minutes in a buffer before functionalization to dissolve the sucrose layer. Then the sensors were dipped for 15 minutes in DNA containing solutions (biotinylated hairpin ODN's) at 100 nM and rinsed in the buffer solution (10 mM HEPES, 50 mM NaCl, 100 mM KCl (pH 7.4), 0.5% v/v surfactant P20) for 10 minutes. The functionalized sensors were next dipped in the ruthenium complex containing solution at different concentrations (see supporting information) for 4 minutes interspersed by a rinsing step in the buffer solution for 4 minutes. Reference sensors without DNA immobilization were used to subtract the non-specific adsorption on the SA layer. The sensorgrams were fit using a 1:1 interaction model. The reported values are the means of representative independent experiments, and the errors provided are standard deviations from the mean. Each experiment was repeated at least two times using a concentration range from 0.5 µM to 150 µM.

Synthetic procedures and characterization

$[Ru(bpy)_2napp]^{2+}$ 1. The $[Ru(bpy)_2Cl_2]$ precursor (20 mg, 0.041 mmol, 1.0 eq.) and napp (20 mg, 0.061 mmol, 1.5 eq) were mixed in a solution of absolute ethanol/water (5/5 - v/v, 5 mL). The reaction mixture was then stirred at 80 °C until the ligand was consumed as monitored by TLC (3 h). Afterwards, ethanol was evaporated and addition of small portions of NH_4PF_6 yielded to the formation of an orange precipitate. After centrifugation,

the solid was washed several times with water and was then dried *in vacuo*. The so formed orange-red crude was finally purified on silica gel chromatography (10:1:0.5 $CH_3CN/H_2O/$ KNO_{3sat}) to afford $[Ru(bpy)_2napp]^{2+}$ **1** as an orange solid (31 mg, 0.030 mmol, 73%). The counter-anion exchange from PF_6^- to Cl^- was performed by adding small portions of NBu_4Cl to a solution of the complex in acetone. R_f 0.35 ($CH_3CN/H_2O/$ KNO_{3sat} 10:1:0.5); ^1H NMR (CD_3CN, 500 MHz) δ (ppm), 10.47 (1H, s, H_d), 9.81 (1H, d, J_{a-b} = 8.2, J_{a-c} = 1.2 Hz, Ha), 9.59 (1H, dd, J_{c-b} = 8.2, J_{c-a} = 1.2 Hz, H_c), 9.24 (1H, d, J_{m-l} = 8.2 Hz, H_m), 8.53 (4H, m, H_5, $H_{5'}$, H_6, $H_{6'}$), 8.34 (1H, d, J_{i-j} = 9.1 Hz, H_i), 8.25 (1H, d, J_{j-i} = 9.1 Hz, H_j), 8.16 (2H, m, H_4, $H_{4'}$), 8.12 (3H, m, H_e, H_f, H_g), 8.01 (2H, m, H_7, $H_{7'}$), 7.95 (1H, m, H_l), 7.91-7.84 (5H, m, H_b, H_2, $H_{2'}$, H_m, H_h), 7.73 (1H, d, J_{9-8} = 5.4 Hz, H_9), 7.69 (1H, d, $J_{9'-8'}$ = 5.6 Hz, $H_{9'}$), 7.49-7.44 (2H, m, H_3, $H_{3'}$), 7.28-7.21 (m, 2H, H_8, $H_{8'}$); HRMS-ESI calculated for $[C_{43}H_{29}N_7F_6PRu]^+$: *m/z* 890.11728, found: *m/z* 890.11700 and for $[C_{43}H_{29}N_7Ru]^{2+}$: *m/z* 372.57617, found: *m/z* 372.57640.

$[Ru(phen)_2cpip]^{2+}$ 2. Using the same procedure as for complex **1** with the precursor $[Ru(phen)_2Cl_2]$ (20 mg, 0.038 mmol) and cpip (15 mg, 0.045 mmol) gave the crude product that was purified by flash chromatography on silica ($CH_3CN/H_2O/$ KNO_{3sat} 10:1:0.25) to provide the title compound **3** as an orange solid (30 mg, 0.025 mmol, 68%). R_f 0.30 ($CH_3CN/H_2O/$ KNO_{3sat} 10:1:0.25); ^1H NMR (CD_3CN, 500 MHz) δ 9.05 (d, 1H, J = 8.2 Hz, H_a /$H_{a'}$), 8.89 (d, 1H, J = 8.4 Hz, H_a /$H_{a'}$), 8.59 (dd, 4H, J = 8.3 Hz, J = 1.2 Hz, H_2/$H_{2'}$ *and* H_9/$H_{9'}$), 8.28 (d, 2H, J = 8.7 Hz, H_e *and* $H_{e'}$), 8.25 (s, 4H, H_5 *and* $H_{5'}$*;* H_6 *and* $H_{6'}$), 8.07 (dd, 2H, J = 10.5 Hz, J = 4.8 Hz, H_8 *and* $H_{8'}$), 8.01 (d, 2H, J = 5.4 Hz, H_7 *and* $H_{7'}$), 7.96 (d, 2H, J = 5.2 Hz, H_4 *and* $H_{4'}$,), 7.67-7.59 (m, 8H, H_3 $H_{3'}$, H_b, $H_{b'}$, H_c, $H_{c'}$, H_d *and* $H_{d'}$). HRMS Calcd for $[C_{43}H_{27}N_8ClF_6PRu]^+$: *m/z* 931.07595, found: *m/z* 931.07688 Da.

$[Ru(phen)_2salphen]^{2+}$ 3. Using the same procedure as for complex **1** with the precursor $[Ru(phen)_2Cl_2]$ (20 mg, 0.038 mmol) and salphen (16 mg, 0.038 mmol) gave the crude product that was purified by flash chromatography on silica ($CH_3CN/H_2O/$ KNO_{3sat} 10:1:0.25) to provide the title compound **2** as an orange solid (33 mg, 0.028 mmol, 75%). R_f 0.31 ($CH_3CN/H_2O/$ KNO_{3sat} 10:1:0.25); ^1H NMR (CD_3CN, 500 MHz) δ 9.03 (broad m, 4H, H_d and H_c), 8.62 – 8.60 (m, 2H, H_2 or H_9), 8.60 – 8.58 (m, 2H, H_2 or H_9), 8.25 (s, 4H, H_5 and H_6), 8.12 – 8.06 (m, 4H, H_7 and H_e), 8.02 (dd, J = 5.2, 1.2 Hz, 2H, H_4), 7.99 (dd, J = 5.3, 1.2 Hz, 2H, H_a), 7.68 (dd, J = 8.3, 5.3 Hz, 2H, H_b), 7.63 (d, J = 5.2 Hz, 2H, H_3 or H_8), 7.61 (d, J = 5.2 Hz, 2H, H_3 or H_8), 7.51 – 7.44 (m, 2H, H_g), 7.17 – 7.06 (m, 4H, H_f and H_h). HRMS-ESI calculated for $[C_{43}H_{28}N_8O^{96}Ru]^{2+}$: *m/z* 384.07255, found: *m/z* 384.07322.

Conflicts of interest

The authors declare no competing interest.

Acknowledgements

M. G. and B. E. gratefully acknowledge the Université catholique de Louvain (UCLouvain) and the F.R.S-FNRS (Grant Number U.N021.21) for financial support. This work was partially supported by the "Agence National de la Recherche", Labex ARCANE (ANR-16-CE11-0006-01), CBH-EUR-GS (ANR-17-EURE-0003), and the région Auvergne-Rhône-Alpes. The NanoBio-ICMG platforms (UAR 2607) are acknowledged for their support.

References

(1) Crosby, D.; Lyons, N.; Greenwood, E.; Harrison, S.; Hiom, S.; Moffat, J.; Quallo, T.; Samuel, E.; Walker, I. A roadmap for the early detection and diagnosis of cancer. *The Lancet Oncology* **2020**, *21* (11), 1397-1399. DOI: https://doi.org/10.1016/S1470-2045(20)30593-3.

(2) Shieh, Y.; Eklund, M.; Sawaya, G. F.; Black, W. C.; Kramer, B. S.; Esserman, L. J. Population-based screening for cancer: hope and hype. *Nature Reviews Clinical Oncology* **2016**, *13* (9), 550-565. DOI: 10.1038/nrclinonc.2016.50.

(3) Katerji, M.; Filippova, M.; Duerksen-Hughes, P. Approaches and Methods to Measure Oxidative Stress in Clinical Samples: Research Applications in the Cancer Field. *Oxid. Med. Cell. Longev.* **2019**, *2019*, 1279250-1279250. DOI: 10.1155/2019/1279250 PubMed.

(4) Møller, P.; Folkmann, J. K.; Forchhammer, L.; Bräuner, E. V.; Danielsen, P. H.; Risom, L.; Loft, S. Air pollution, oxidative damage to DNA, and carcinogenesis. *Cancer Lett.* **2008**, *266* (1), 84-97. DOI: https://doi.org/10.1016/j.canlet.2008.02.030. Ames, B. N.; Shigenaga, M. K.; Hagen, T. M. Oxidants, antioxidants, and the degenerative diseases of aging. *Proceedings of the National Academy of Sciences* **1993**, *90* (17), 7915-7922. DOI: doi:10.1073/pnas.90.17.7915. Nakabeppu, Y.; Sakumi, K.; Sakamoto, K.; Tsuchimoto, D.; Tsuzuki, T.; Nakatsu, Y. Mutagenesis and carcinogenesis caused by the oxidation of nucleic acids. **2006**, *387* (4), 373-379. DOI: doi:10.1515/BC.2006.050. Pizzino, G.; Irrera, N.; Cucinotta, M.; Pallio, G.; Mannino, F.; Arcoraci, V.; Squadrito, F.; Altavilla, D.; Bitto, A. Oxidative Stress: Harms and Benefits for Human Health. *Oxid. Med. Cell. Longev.* **2017**, *2017*, 8416763. DOI: 10.1155/2017/8416763.

(5) Ludlow, A. T.; Spangenburg, E. E.; Chin, E. R.; Cheng, W.-H.; Roth, S. M. Telomeres shorten in response to oxidative stress in mouse skeletal muscle fibers. *The journals of gerontology. Series A, Biological sciences and medical sciences* **2014**, *69* (7), 821-830. DOI: 10.1093/gerona/glt211 PubMed. Barnes, R. P.; Fouquerel, E.; Opresko, P. L. The impact of oxidative DNA damage and stress on telomere homeostasis. *Mech. Ageing Dev.* **2019**, *177*, 37-45. DOI: https://doi.org/10.1016/j.mad.2018.03.013. von Zglinicki, T. Oxidative stress shortens telomeres. *Trends Biochem Sci* **2002**, *27* (7), 339-344. DOI: 10.1016/s0968-0004(02)02110-2 From NLM.

(6) Ahmed, W.; Lingner, J. Impact of oxidative stress on telomere biology. *Differentiation* **2018**, *99*, 21-27. DOI: https://doi.org/10.1016/j.diff.2017.12.002. Dewhurst, S. M. Chromothripsis and telomere crisis: engines of genome instability. *Curr. Opin. Genet. Dev.* **2020**, *60*, 41-47. DOI: https://doi.org/10.1016/j.gde.2020.02.009.

(7) Steenken, S.; Jovanovic, S. V. How Easily Oxidizable Is DNA? One-Electron Reduction Potentials of Adenosine and Guanosine Radicals in Aqueous Solution. *J. Am. Chem. Soc.* **1997**, *119* (3), 617-618. DOI: 10.1021/ja962255b.

(8) Fouquerel, E.; Barnes, R. P.; Uttam, S.; Watkins, S. C.; Bruchez, M. P.; Opresko, P. L. Targeted and Persistent 8-Oxoguanine Base Damage at Telomeres Promotes Telomere Loss and Crisis. *Mol. Cell* **2019**, *75* (1), 117-130.e116. DOI: https://doi.org/10.1016/j.molcel.2019.04.024.

(9) Nakabeppu, Y. Cellular Levels of 8-Oxoguanine in either DNA or the Nucleotide Pool Play Pivotal Roles in Carcinogenesis and Survival of Cancer Cells. *Int. J. Mol. Sci.* **2014**, *15* (7), 12543-12557. Manavalan, S.; Rajaji, U.; Chen, S.-M.; Steplin Paul Selvin, S.; Govindasamy, M.; Chen, T.-W.; Ajmal Ali, M.; Al-Hemaid, F. M. A.; Elshikh, M. S. Determination of 8-hydroxy-2′-deoxyguanosine oxidative stress biomarker using dysprosium oxide nanoparticles@reduced graphene oxide. *Inorganic Chemistry Frontiers* **2018**, *5* (11), 2885-2892, 10.1039/C8QI00727F. DOI: 10.1039/C8QI00727F. Kang, D. M.; Shin, J.-I.; Kim, J. B.; Lee, K.; Chung, J. H.; Yang, H.-W.; Kim, K.-N.; Han, Y. S. Detection of 8-oxoguanine and apurinic/apyrimidinic sites using a fluorophore-labeled probe with cell-penetrating ability. *BMC Molecular and Cell Biology* **2019**, *20* (1), 54. DOI: 10.1186/s12860-019-0236-x. Chiorcea-Paquim, A.-M. 8-oxoguanine and 8-oxodeoxyguanosine Biomarkers of Oxidative DNA Damage: A Review on HPLC–ECD Determination. *Molecules* **2022**, *27* (5), 1620.

(10) Bochman, M. L.; Paeschke, K.; Zakian, V. A. DNA secondary structures: stability and function of G-quadruplex structures. *Nature Reviews Genetics* **2012**, *13* (11), 770-780. DOI: 10.1038/nrg3296. Burge, S.; Parkinson, G. N.; Hazel, P.; Todd, A. K.; Neidle, S. Quadruplex DNA: sequence, topology and structure. *Nucleic Acids Res.* **2006**, *34* (19), 5402-5415. DOI: 10.1093/nar/gkl655 From NLM.

(11) Miclot, T.; Corbier, C.; Terenzi, A.; Hognon, C.; Grandemange, S.; Barone, G.; Monari, A. Forever Young: Structural Stability of Telomeric Guanine Quadruplexes in the Presence of Oxidative DNA Lesions**. *Chem. Eur. J.* **2021**, *27* (34), 8865-8874, https://doi.org/10.1002/chem.202100993. DOI: https://doi.org/10.1002/chem.202100993 (acccessed 2022/01/24). Bielskutė, S.; Plavec, J.; Podbevšek, P. Oxidative lesions modulate G-quadruplex stability and structure in the human BCL2 promoter. *Nucleic Acids Res.* **2021**, *49* (4), 2346-2356. DOI: 10.1093/nar/gkab057 (acccessed 11/5/2021). Singh, A.; Kukreti, R.; Saso, L.; Kukreti, S. Oxidative Stress: Role and Response of Short Guanine Tracts at Genomic Locations. *Int. J. Mol. Sci.* **2019**, *20* (17), 4258.

(12) Bielskutė, S.; Plavec, J.; Podbevšek, P. Impact of Oxidative Lesions on the Human Telomeric G-Quadruplex. *J. Am. Chem. Soc.* **2019**, *141* (6), 2594-2603. DOI: 10.1021/jacs.8b12748.

(13) Friedman, A. E.; Chambron, J. C.; Sauvage, J. P.; Turro, N. J.; Barton, J. K. A molecular light switch for DNA: Ru(bpy)2(dppz)2+. *J. Am. Chem. Soc.* **1990**, *112* (12), 4960-4962. DOI: 10.1021/ja00168a052. Smith, J. A.; Collins, J. G.; Keene, F. R. Groove-Binding Ruthenium(II) Complexes as Probes of DNA Recognition. In *Metal Complex–DNA Interactions*, John Wiley & Sons, Ltd, 2009; pp 317-346. McConnell, A. J.; Lim, M. H.; Olmon, E. D.; Song, H.; Dervan, E. E.; Barton, J. K. Luminescent Properties of Ruthenium(II) Complexes with Sterically Expansive Ligands Bound to DNA Defects. *Inorganic Chemistry* **2012**, *51* (22), 12511-12520. DOI: 10.1021/ic3019524. Wachter, E.; Moyá, D.; Parkin, S.; Glazer, E. C. Ruthenium Complex "Light Switches" that are Selective for Different G-Quadruplex Structures. *Chem. Eur. J.* **2016**, *22* (2), 550-559. DOI: 10.1002/chem.201503203. Piraux, G.; Bar, L.; Abraham, M.; Lavergne, T.; Jamet, H.; Dejeu, J.; Marcélis, L.; Defrancq, E.; Elias, B. New Ruthenium-Based Probes for Selective G-Quadruplex Targeting. *Chem. Eur. J.* **2017**, *23*, 11872-11880. DOI: 10.1002/chem.201702076. Boynton, A. N.; Marcélis, L.; McConnell, A. J.; Barton, J. K. A Ruthenium(II) Complex as a Luminescent Probe for DNA Mismatches and Abasic Sites. *Inorganic Chemistry* **2017**, *56* (14), 8381-8389. DOI: 10.1021/acs.inorgchem.7b01037. Gill, M. R.; Thomas, J. A. Ruthenium(ii) polypyridyl complexes and DNA-from structural probes to cellular imaging and therapeutics. *Chem. Soc. Rev.* **2012**, *41* (8), 3179-3192, 10.1039/C2CS15299A. DOI: 10.1039/C2CS15299A. Gill, M. R.; Garcia-Lara, J.; Foster, S. J.; Smythe, C.; Battaglia, G.; Thomas, J. A. A ruthenium(II) polypyridyl complex for direct imaging of DNA structure in living cells. *Nat. Chem.* **2009**, *1* (8), 662-667. DOI:

10.1038/nchem.406 From NLM. Berrones Reyes, J.; Kuimova, M. K.; Vilar, R. Metal complexes as optical probes for DNA sensing and imaging. *Curr. Opin. Chem. Biol.* **2021**, *61*, 179-190. DOI: https://doi.org/10.1016/j.cbpa.2021.02.007. Jiang, J.; Teunens, T.; Tisaun, J.; Denuit, L.; Moucheron, C. Ruthenium(II) Polypyridyl Complexes and Their Use as Probes and Photoreactive Agents for G-quadruplexes Labelling. *Molecules* **2022**, *27* (5), 1541. Gillard, M.; Piraux, G.; Daenen, M.; Abraham, M.; Troian-Gautier, L.; Bar, L.; Bonnet, H.; Loiseau, F.; Jamet, H.; Dejeu, J.; et al. Photo-oxidizing Ruthenium(II) Complexes with Enhanced Visible Light Absorption and G-quadruplex DNA Binding Abilities. *Chem. Eur. J.* **2022**, *n/a* (n/a). DOI: https://doi.org/10.1002/chem.202202251.

(14) Deraedt, Q.; Marcelis, L.; Loiseau, F.; Elias, B. Towards mismatched DNA photoprobes and photoreagents: "elbow-shaped" Ru(ii) complexes. *Inorg. Chem. Front.* **2017**, *4* (1), 91-103, 10.1039/C6QI00223D. DOI: 10.1039/C6QI00223D.

(15) Weynand, J.; Diman, A.; Abraham, M.; Marcélis, L.; Jamet, H.; Decottignies, A.; Dejeu, J.; Defrancq, E.; Elias, B. Towards the Development of Photo-Reactive Ruthenium(II) Complexes Targeting Telomeric G-Quadruplex DNA. *Chem. Eur. J.* **2018**, *24* (72), 19216-19227. DOI: doi:10.1002/chem.201804771.

(16) Gillard, M.; Weynand, J.; Bonnet, H.; Loiseau, F.; Decottignies, A.; Dejeu, J.; Defrancq, E.; Elias, B. Flexible RuII Schiff Base Complexes: G-Quadruplex DNA Binding and Photo-Induced Cancer Cell Death. *Chem. Eur. J.* **2020**, *26* (61), 13849-13860, https://doi.org/10.1002/chem.202001409. DOI: https://doi.org/10.1002/chem.202001409 (acccessed 2021/02/08). Gillard, M.; Laramée-Milette, B.; Deraedt, Q.; Hanan, G. S.; Loiseau, F.; Dejeu, J.; Defrancq, E.; Elias, B.; Marcélis, L. Photodetection of DNA mismatches by dissymmetric Ru(ii) acridine based complexes. *Inorg. Chem. Front.* **2019**, *6* (9), 2260-2270. DOI: 10.1039/C9QI00133F.

(17) Amouyal, E.; Homsi, A.; Chambron, J.-C.; Sauvage, J.-P. Synthesis and study of a mixed-ligand ruthenium(II) complex in its ground and excited states: bis(2,2[prime or minute]-bipyridine)(dipyrido[3,2-a : 2[prime or minute],3[prime or minute]-c]phenazine-N4N5)ruthenium(II). *Journal of the Chemical Society, Dalton Transactions* **1990**, (6), 1841-1845, Article Journal.

(18) Deraedt, Q.; Marcélis, L.; Auvray, T.; Hanan, G. S.; Loiseau, F.; Elias, B. Design and Photophysical Studies of Acridine-Based RuII Complexes for Applications as DNA Photoprobes. *Eur. J. Inorg. Chem.* **2016**, *2016* (22), 3649-3658. DOI: 10.1002/ejic.201600468.

(19) Brouwer, A. M. Standards for photoluminescence quantum yield measurements in solution (IUPAC Technical Report). *Pure and Applied Chemistry* **2011**, *83* (12), 2213-2228.

(20) McGhee, J. D.; von Hippel, P. H. Theoretical aspects of DNA-protein interactions - Cooperative and non-cooperative binding of large ligands to a one-dimensional homogeneous lattice. *J. Mol. Biol.* **1974**, *86*, 469-489. DOI: 10.1016/0022-2836(74)90031-x.

(21) Wallner, J.; Lhota, G.; Jeschek, D.; Mader, A.; Vorauer-Uhl, K. Application of Bio-Layer Interferometry for the analysis of protein/liposome interactions. *Journal of Pharmaceutical and Biomedical Analysis* **2013**, *72*, 150-154. DOI: https://doi.org/10.1016/j.jpba.2012.10.008. Picault, L.; Laigre, E.; Gillon, E.; Tiertant, C.; Renaudet, O.; Imberty, A.; Goyard, D.; Dejeu, J. Characterization of the interaction of multivalent glycosylated ligands with bacterial lectins by biolayer interferometry. *Glycobiology* **2022**, *32* (10), 886-896. DOI: 10.1093/glycob/cwac047 (acccessed 9/28/2022).

Table of Contents